µ-PIV and ELDV wind tunnel investigations of the laminar separation bubble above a helicopter blade tip

M. Raffel, D. Favier, E. Berton, C. Maresca, C. Rondot, M. Nsimba, W. Geissler

Abstract Detailed studies of the boundary layer profile and the characteristics of the flow velocity distribution close to the leading edge of a helicopter blade profile were conducted using the embedded laser doppler velocimetry (ELDV) and stereo-PIV. The relatively small scales of flow structures related to dynamic stall, motivated an additional 2C-PIV study in which the flow field has been measured with a relatively high spatial resolution. The feasibility of PIV measurements utilizing a mirror telescope in a wind tunnel has been demonstrated successfully. The spatial resolution of approximately 50 µm allowed a judgment on the choice of turbulence models and damping coefficients for the improvement of CFD predictions.

1
Introduction

Over the past decade, considerable progress has been made in the development of performance prediction capabilities for isolated helicopter components. Modern CFD methods deliver promising results for moderate operation conditions. The prediction of high speed and high load cases still needs more intensive experimental investigations of the unsteady viscous flow phenomena, such as the dynamic stall at the retreating side of the rotor and the complex mechanism of the stall in the vicinity of the blade tip. Overall flow field measurements on pitching airfoils, pitching finite blade models and on rotating blades in hover chambers and wind tunnels have been successfully performed at different places.

The dynamic stall process, which is limiting the forward flight speed, is characterized in almost all cases by the formation of a strong vortex at the leading edge of the blade profile. The circulation of this vortex, which stays attached to the model for a relative long time of the cycle, is responsible for the - compared to the steady case - significant increase in lift and drag coefficient. However, its convection over the upper surface of the blade needs to be avoided, since it generates strong pitching moment variations resulting in vibrations and high mechanical loads (McCroskey et al. 1982). Earlier investigations proofed the existence of a small flow regime, which dominates the leading edge stall at pitching airfoils at higher Mach and Reynolds numbers (Geißler et al. 1998). Furthermore, it has been found by numerical as well as experimental investigations, (Geißler et al. 2004), that free transition of the flow from laminar to turbulent may play a dominant role with respect to unsteady flow characteristics. In particular at low Reynolds numbers ($<10^5$) transition develops over a major part of the airfoil upper surface during the oscillatory motion. The effects of transition on dynamic stall characteristics are then no longer negligible. Laser based flow visualization and anemometry has therefore been used for the qualitative description of the phenomenon and a more detailed comparison with numerical simulation of the transition and the further development of the stall process. PIV investigations have been performed at different reduced frequencies, positions and spatial resolutions. In this article we mainly focus on measurements, which have been obtained for a steady incidence angle of 11.5°, since the flow phenomena involved are best understood and documented. This incidence angle corresponds to the point where maximum lift is obtained, shortly below the incidence angle where massive flow separation occurs. The flow around the OA209 profile for this range of Reynolds number, span wise location and incidence angle is determined by the transition of the boundary layer and the flow separation on the suction side which results in the generation of vorticity dominating the wake flow and the performance of the wing. This holds in a similar way for finite wings and 2D-airfoil profiles.

For the present case of moderate Reynolds numbers and high incidence angles, laminar flow separation occurs shortly behind the leading edge and transition to turbulent flow conditions occurs immediately after separation. The resulting turbulence intensity forces a reattachment of the flow within a short distance, resulting in a significantly increased maximum lift with respect to the low Reynolds number cases. The separation together with the re-

M. Raffel[1], D. Favier[2], E. Berton[2], C. Maresca[2], C. Rondot[2], M. Nsimba[2], W. Geissler[1]
1) Deutsches Zentrum für Luft- und Raumfahrt (DLR), Institut für Aerodynamik und Strömungstechnik, Bunsenstr. 10 37073 Göttingen, Germany
2) CNRS, Laboratoire d´Aerodynamique et de Biomechanique du Movement LABM, 163, avenue de Luminy, 13288 Marseille Cedex 09, France

Correspondence to:
M. Raffel, E-mail: markus.raffel@dlr.de

attachment forms a laminar separation bubble containing a recirculation region, which has only a few millimeter extension in chord wise direction (see Fig.1). The turbulent boundary layer behind the bubble allows the flow to stay attached even at relatively high adverse pressure gradients.
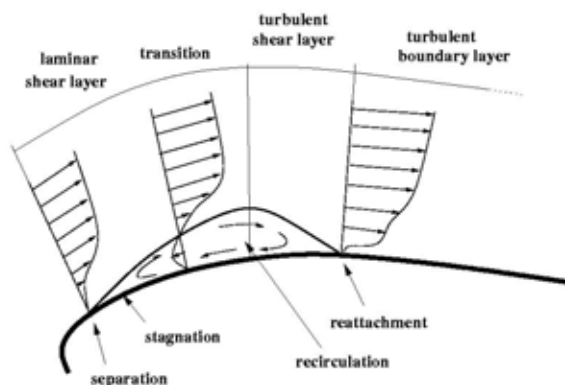

Figure 1: Sketch of the separation bubble

Detailed investigations of the turbulence intensity, the size and the temporal development of the flow structure at the leading edge are required in order to validate CFD-codes which are under development for a more accurate prediction of the dynamic stall cases. Therefore, stereoscopic PIV and pressure measurements have been performed to quantize the overall flow features close to the tip of a rotor blade, both in steady cases and during pitching motion. Two-components PIV measurements with an observation field size of 4 cm x 5 cm and 1.0 mm x 1.2 mm with 1mm and 50 μm resolution respectively, have been performed further inboard in order to resolve the relevant flow features in the phase shortly before the stall onset in steady and unsteady cases. The results of the steady case have been compared with ELDV and CFD data and are described in more detail in the following.

2

Numerical Simulations

The numerical studies in the present report have been carried out with a 2D unsteady Navier-Stokes code. This code uses the Approximate Factorization Implicit methodology originally developed by Beam and Warming (1978). The computations are carried out in a space fixed frame of reference, i.e. the curvilinear coordinates are fixed to the moving body as well as to the static outer frame. This arrangement needs the determination of a new grid for every time-step. These intermediate grids are obtained from the two grids in the extreme (minimum and maximum) incidence conditions by simple linear interpolation. The grids are of C-grid topology. The reason for choosing this procedure is the application of the present tools also for unsteady body deformations, i.e. for airfoils with leading or trailing edge flap motions, etc.

The code has a steady component, which allows the calculation of steady flow data as obtained after a sufficient number of time-steps. The steady version of the code is also working in the time-accurate mode.

Turbulence modeling: Different turbulence models have been implemented in the numerical code and have been tested for their applicability in different flow cases. For dynamic stall flow cases it has been shown that the Spalart-Allmaras (SA) one equation model (Spalart and Allmaras 1992), gives the most reliable results compared to experimental data. In addition the k-ω-SST model (Menter 1992), is also available. This two-equation model shows good results during the upstroke motion prior to severe separation however once separation occurs the model shows unrealistic high hysteresis effects including strong oscillations in the force and moment hysteresis loops. In the present investigation the SA and the k-ω-SST model have been used. An important main test case for the choice of the turbulence model is the prediction of the laminar separation bubble.

3

Embedded Laser Doppler Velocimetry ELDV

The Embedded Laser Doppler Velocimeter (ELDV) used for this survey in 2D flow has an optical head mounted on a supporting turntable linked to the oscillating frame as sketched in Figure 2. Moreover, it is equipped with a beam-

expander to increase the focal distance to 400mm (Berton et al. 2001). This optical head is installed on an automated 2D-displacement device mounted itself on the turntable. The laser beams are focusing via a 45° mirror in the boundary layer at a defined span wise location. The supporting turntable is linked with the oscillating frame, so that U and V velocity components can be directly measured in the same reference frame as the oscillating blade. A remotely driven system allows the adequate positioning of the measurement volume at any point of the airfoil surface (30cm in chord wise displacement). An angular sector provides the selection of the surveying normal direction, and the laser measurement volume can be displaced along the local normal to the surface with a displacement accuracy of 0.1mm. Each velocity component is recorded at each phase angle ωt ranging from 0° to 360° by steps of 1° over a large number of periods. Data are then statistically analyzed at prescribed values of the period, e.g. the instantaneous incidence, with an accuracy of $\delta\alpha=4\Delta\alpha/360=24/360=0.066°$. The acquisition time is stopped when 19,564 data have been stored, that generally requires about 150 periods.
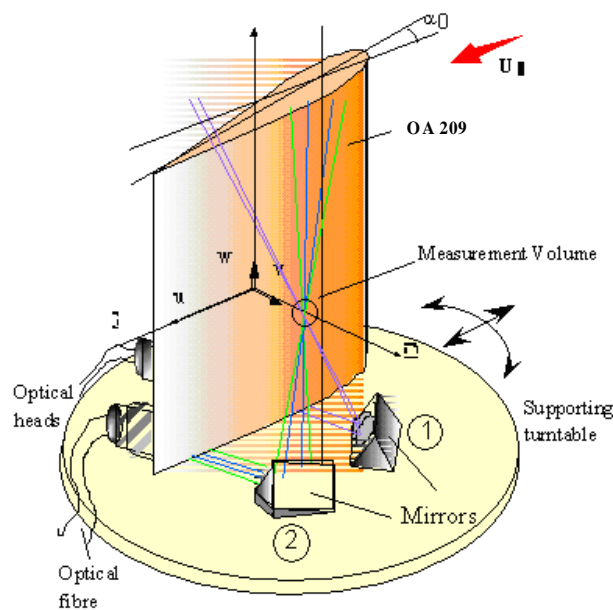

Figure 2: ELDV Set-up

4
Particle Image Velocimetry PIV

The Quantel laser system used had 2 x 200 mJ pulse energy at 532 um and was equipped with conventional light sheet optics as shown in Figure 3. The PCO cameras had a resolution of 1280 x 1024 pixels. Nikon 35mm lenses have been used for the stereoscopic measurements and a conventional Zeiss lens with 100 mm focal length has been used for a more detailed investigation at the leading edge. Additionally, measurements with a telescope lens have been performed in order to resolve the relevant flow features in the phase shortly before the stall onset. The light sheet thickness was around 400 μm during the tests with the 100mm lens. The particle image diameters observed at this resolution varied between 12 μm and 20 μm (2 -3 pixel). The image quality obtained, allowed the analysis of the unsteady flow features at a spatial resolution of ~1 mm.

The set-up used for the PIV measurements with a very high resolution is similar to the one described by Lindken et al. (2002), but has been used under relatively rough conditions in a wind tunnel. The microscope lens used for the test was a mirror objective lens QM100 of Questar Corporation. It is optimized for working distances G, ranging from G = 150 mm to G = 380 mm. It has an aperture angle of Ω = arctg (D / 2G) with D being the aperture diameter. The numerical aperture for the working distance of G = 355 mm, which has been chosen for the experiment, is A = n sinΩ = 0.083 with n being the refractive index of air. The F-number was f# = 1 / 2A = 6 and the magnification M = 4.86 resulting in a calibration factor of 754 px / mm. The diffraction limited minimum image diameter was d_{diff} = 2.44 f# (M+1) λ = 45.6 μm and the estimated depth of focus δ_Z = 2 f# d_{diff} (M+1) / M^2 = 136 μm. The light sheet

thickness was again around 400 μm. Particle image diameters observed where between 50 μm and 130 μm (8 -20 pixel). The development of the boundary layer, the reverse flow region and the shear layer towards the outer flow can clearly be seen in the results shown in the next chapter.
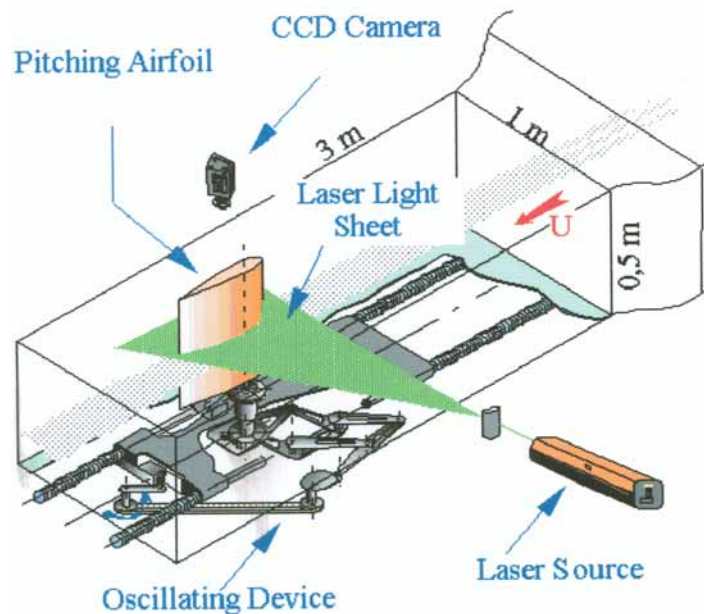

Figure 3: PIV Set-up

5
Test Parameters

The experiments have been performed in the S2 Luminy wind tunnel of the Laboratoire d´Aerodynamique et de Biomechanique du Movement LABM of the French research center CNRS at the University of Marseille. The PIV measurements were performed close to the leading edge of an OA209 blade tip model, in a plane orthogonal to the span in a distance of approximately 200mm. Stereoscopic PIV measurements proofed that the flow at small and moderate incidence angles at this span-wise location is basically two-dimensional and can therefore well be compared with measurement taken at 2D airfoil profiles (see Fig. 4).
The selected airfoil motion for the dynamic investigations had the following incidence law:

Incidence Variation: $\alpha(t) = 11° + 6° \sin (2 \pi f t)$
Reduced Frequency: $k = \pi f c/U_\infty = 0.18 (\omega*=0.36)$
Profile**:**   OA209
Reynolds number: $Re = 0.7 \times 10^5$
Mach number: $M=0.045.$[1]
Mean velocity: $U_\infty=10m/s$
Airfoil chord: $c=0.2m$

The incidence variation of ±6°, the mean incidence of 11° and the reduced frequency of k = 0.18 correspond to the "deep stall" case according to the description given by McCroskey et al. (1982). Under these conditions, strong unsteady effects can be expected and the test case was found to be best suited for a comparison with flow phenomena predicted by numerical simulations.
The majority of the μPIV measurement has been made at a steady incidence angle of 11.5° and has been compared with CFD and ELDV results at the same condition.

---

[1] The Mach number is a necessary input parameter for the numerical code and is set to a small number to simulate definitely incompressible flow.

6
Results and Discussion

In order to follow the evolution of the dynamic stall process and to study the variation from cycle to cycle in a conclusive way, more than 100 different PIV recordings were taken and evaluated for each set of parameters. From the amount of data, only a few records concerning the three main features of the investigated flow, i.e. existence of attached flow at high incidences, development of the dynamic stall vortex and its two-dimensionality have been presented next. Results from the measurement of the laminar separation bubble are shown and discussed further below.

In the steady case, the first indications of stall were observed at an incidence of $\alpha \approx 12°$. A separated flow with weakly formed vortices within the shear layer is then seen at $\alpha = 14.4°$ (Fig. 4, right). In Figure 4 and 5, the out-of-plane velocity component W has been normalized with the magnitude of the free stream velocity. The coordinates x and y have been normalized with the chord length and the origin is located on the axis of rotation.
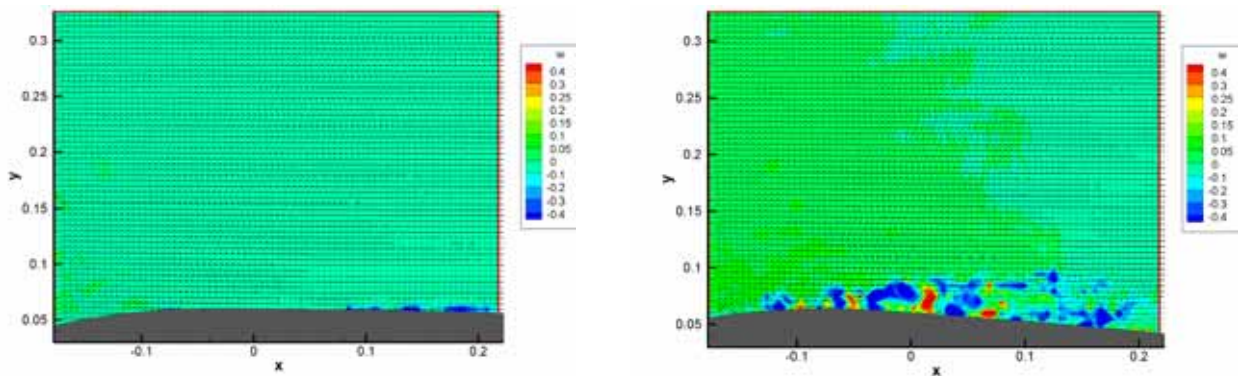

Figure 4: Stereo-PIV results of $\alpha = 9.8°$ (left) and $\alpha = 14.4°$ (right); **steady case**.

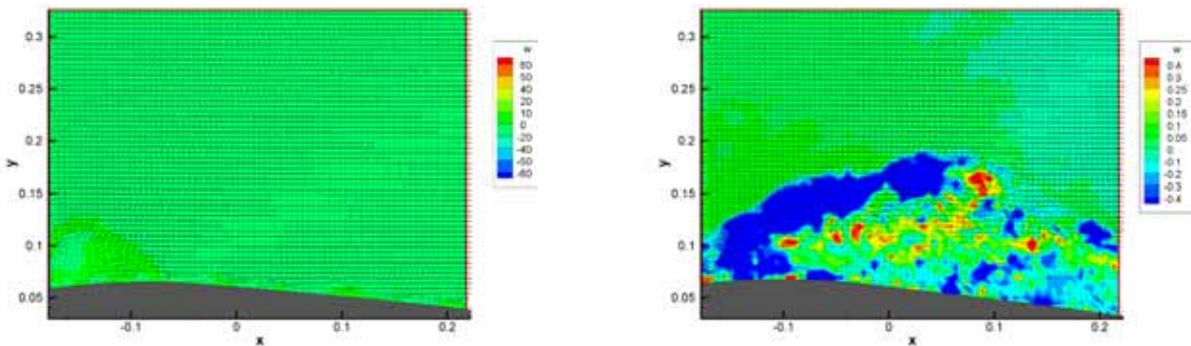**Figure 5:** Stereo-PIV results at $\alpha = 14.8°$ (left) and $\alpha = 16.3°$ (right); **pitching blade** in up-stroke motion.

When the airfoil oscillates as described in section 5, the flow is still fully attached even at incidence angles above $\alpha = 12° \uparrow$ ($\uparrow$ is the sign of the up-stroke motion). One of the major features of dynamic stall - delay of stall to higher incidences - appears clearly. As the incidence increases, the dynamic stall vortex formed at the airfoil leading edge, grows and moves downstream. At $\alpha = 14.8° \uparrow$, the dynamic stall vortex extends over about 25% of the upper surface of the airfoil (Fig. 5, left). Up to this point the flow stays more or less two-dimensional. At $\alpha = 16.3° \uparrow$ a strong spatial variation of the out-of-plane velocity distribution (see Fig. 5, right) occurs when the flow separates. At this phase of the pitching motion, the PIV data reveal a random like distribution of intense small-scale vortical structures inside the dynamic stall vortex. These three-dimensional effects especially during this phase of the process are neglected in most experimental and numerical simulations dealing with 2d airfoils. The later comparison of results obtained at finite blade models (PIV) with results obtained at 2d-airfoils (ELDV and CFD) is restricted to smaller incidence angle where no massive flow separation occurs. For the demonstration of the different observation field sizes and resolutions obtained the color coded flow velocity fields measured by PIV are presented in the

following. The observation field scaled in size and location with respect to the model contour is shown on the left hand side. The magnitude of the velocity has been normalized with the magnitude of the free stream velocity. The coordinates x and y have been normalized with the cord length and the origin is placed on the axis of rotation.
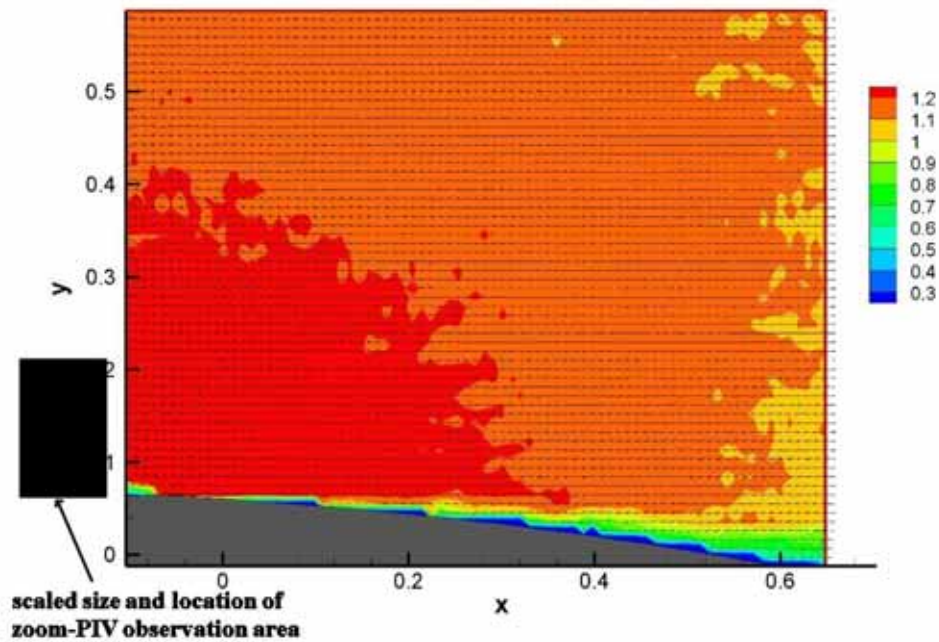

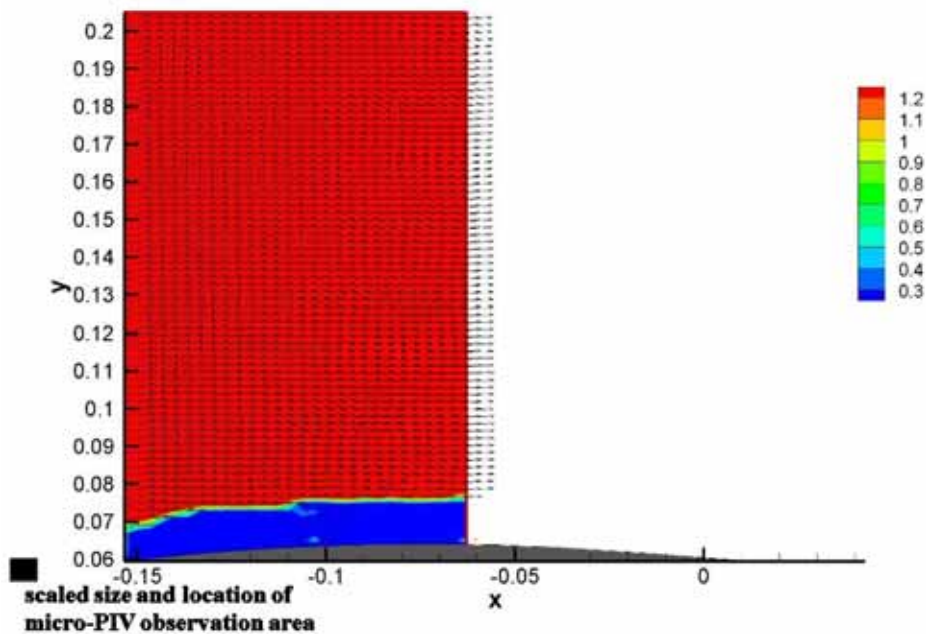**Figure 6**: Stereo PIV results obtained with two 35mm lenses at α = 11.5°, **steady case.**

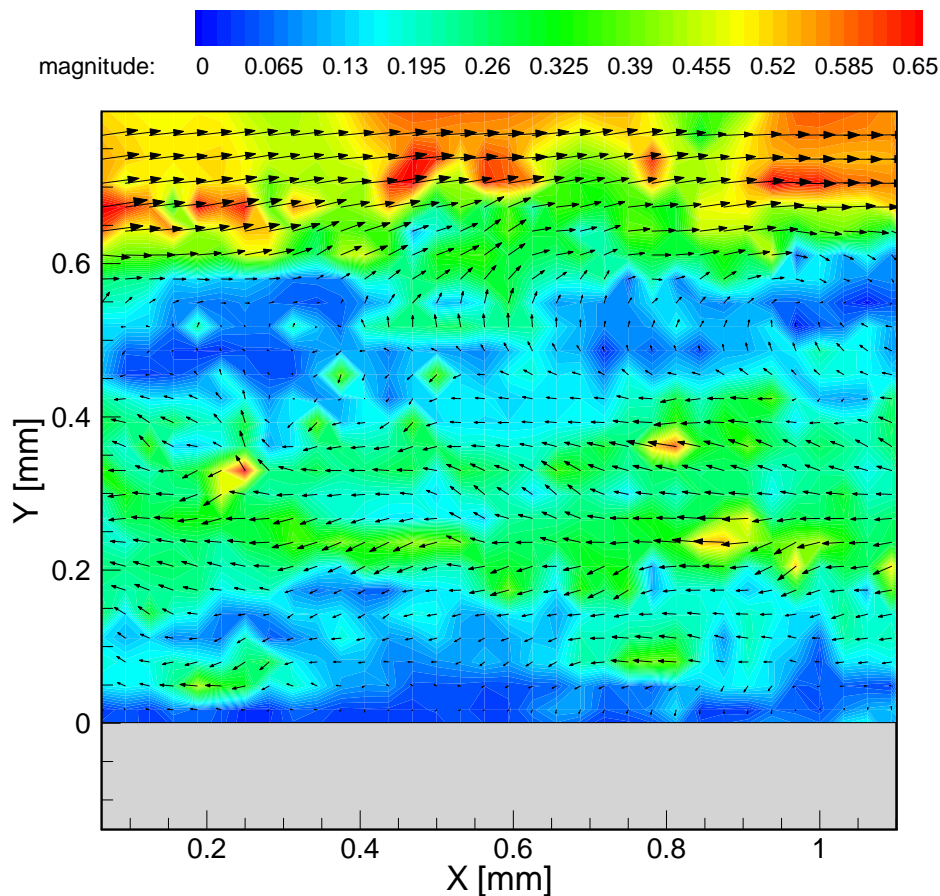**Figure 7: "Zoom-PIV"** results obtained with a 100mm lens at α = 11.5°, **steady case.**

Figure 8: "**µ-PIV**" results obtained with a mirror telescope objective at α = 11.5°, **steady case.**
The magnitude of the velocity has been plotted color coded (color units: c/s). The coordinates *x* and *y* are given in millimeters. The origin is placed on the model surface (y), 5% chord length behind the leading edge (x).

The image quality obtained with the mirror telescope objective, allowed the analysis of the unsteady flow features at a spatial resolution of ~ 50 µm. The number of outliers was in the order of 5%. The relative accuracy compared to the conventional PIV recordings shown previously, was slightly lower due to the fact that the particle images were app. 5 times larger. However, the uncertainty due to noise is assumed to be in the order of 0.1 m/s and the wall distance of each measurement location can very precisely be determined, since the surface is visible in each recording. Therefore, the development of the boundary layer, the reverse flow region and the shear layer towards the outer flow can clearly be seen in the result shown in Figure 8.
Figures 9 and 10 show tangential velocity profiles through the laminar separation bubble obtained by CFD with SA- and SST turbulence model and by ELDV, PIV and µPIV. It can be seen that the agreement of most of the different methods in the outer regions (20mm and above) is relatively high (~98% with respect to the free stream velocity). However, the more detailed presentation in figure 10 shows that the differences between the different experimental results as well as of the different CFD results can easily be seen. The reason for the differences of the PIV and the µPIV results can easily be explained by the weak spatial resolution of the recordings made with the 100mm lens. The differences between the ELDV measurements and the µPIV measurements are more significant and differ not as much in the measured flow velocity, but in the size of the separation bubble in wall normal direction. One reason for this might be a small disagreement of the incidence angle adjustment of both tests. However the conclusion which turbulence model resolves the flow field in the separation bubble best, can easily are drawn in favor for the SA-turbulence model.
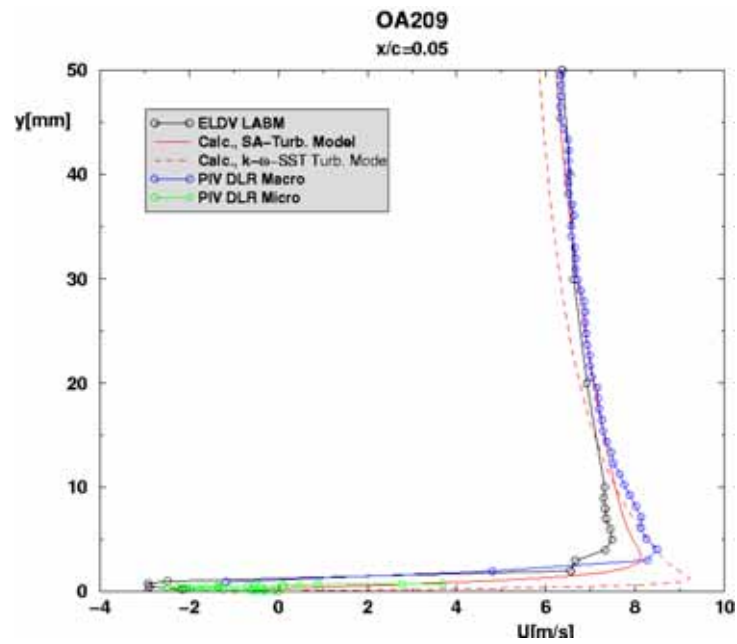
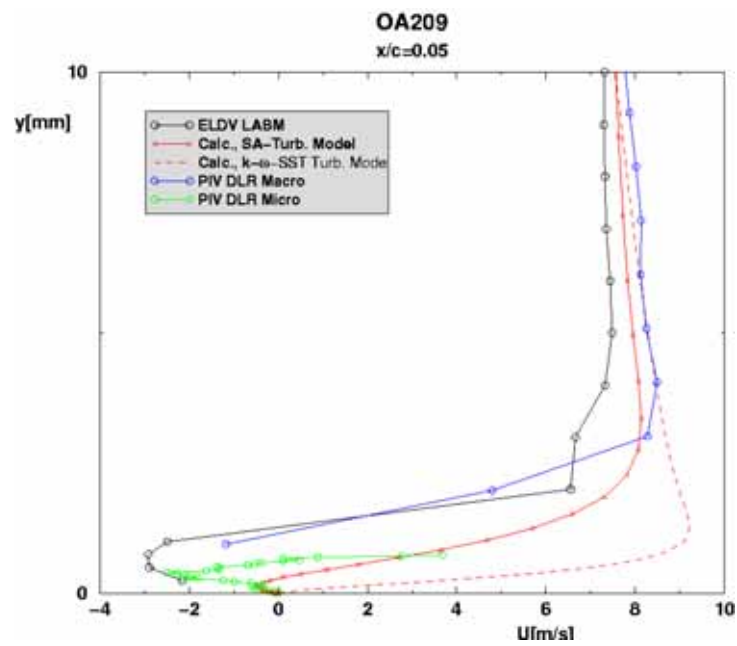**Figure 9:** CFD, ELDV and PIV results of the laminar separation bubble at α = 11.5°; **steady case**.

Figure 10: CFD, ELDV and PIV results of the laminar separation bubble at α = 11.5°; **steady case**.

5 Conclusions

The unsteady flow field above a OA209 blade tip at steady as well as at deep dynamic stall conditions has been investigated in a low-speed wind tunnel by means of the particle image velocimetry. The velocity fields - partly measured with a very high spatial resolution - show small scale structures in the separation bubble. The results have been compared with ELDV data and CFD data. Discrepancies concerning the size of the separation bubble have been observed as well as an acceptable agreement of the velocity magnitudes found by the different measurements. Nevertheless, the present results can be considered to be a good data basis for the validation of numerical codes. However, the finely structured vortices observed at high incidences and their complex evolution during some phases of the pitching is not yet sufficiently predicted by two-dimensional computations. It has been demonstrated that instantaneous velocity fields determined by PIV at high spatial resolutions can be used to choose turbulence models and numerical damping coefficients. The strength, scale, and distribution of the laminar separation bubble - measured for the first time with such a high resolution in a wind tunnel experiment - are essential for the validation of numerical simulation techniques.

References

Geißler,W.,Dietz,G.,Mai,H.,Junker,B.,Lorkowski,T. (2004) "Dynamic Stall Control Investigations on a Full Size Chord Blade Section", 30th European Rotorcraft Forum, Marseille,France, 14.-16.9.
McCroskey,W.J., McAlister K.W.,Carr L.W.,Pucci S.L. (1982) "An Experimental Study of Dynamic Stall on Advanced Airfoil Sections", NASA TM-84245, Vol.1, 2, 3.
Geißler,W.,Carr,L.W.,Chandrasekhara,M.S.,Wilder,M.C.,Sobieczky,H. (1998) "Compressible Dynamic Stall Calculations Incorporating Transition Modelling for Variable Geometry Airfoils",36th AIAA Aerospace Meeting and Exhibit, January, 12-15., Reno, NV.
Beam,R.,Warming,R.F. (1978) "An Implicit Factored Scheme for the Compressible Navier-Stokes Equations",AIAA Journal, Vol.6, No.4.
Spalart,P.R.,Allmaras,S.R. (1992) "A One Equation Turbulence Model for Aerodynamic Flows", AIAA-paper 92-0439.
Menter,F.R. (1992) "Improved Two-Equation k-ω-Turbulence Models for Aerodynamic Flows", NASA TM-103975.
Berton E., Favier D., Nsi Mba M., Maresca C., Allain C. (2001) "Embedded LDV measurements methods applied to unsteady flows investigation", Experiments in Fluids, Vol. 30, n° 1, pp. 102-110
Lindken, R.; Di Silvestro, F.; Westerweel, J.; Nieuwstadt, F. (2002) "Turbulence measurements with μ-PIV in large-scale pipe flow.", Proceedings of the 11th International Symposium Applications of Laser Techniques to Fluid Mechanics, Lisbon, Portugal, paper 12.1.

Acknowledgements